Proceedings of 5th Jagiellonian Symposium on Advances in Particle Physics and Medicine, Kraków, Poland, 2024

Study of Mechanisms of Positronium Formation on Metal Surfaces

J. Čížek* and O. Melikhova

Faculty of Mathematics and Physics, Charles University, V Holešovičkách 2, 18000, Praha 8, Czech Republic

Doi: 10.12693/APhysPolA.146.693 *e-mail: jakub.cizek@mff.cuni.cz

A magnetically guided variable-energy slow-positron beam was used to investigate the formation of positronium on untreated metal surfaces by measuring the annihilation ratio of 3γ to 2γ. The results indicated that positronium formation occurs exclusively at incident positron energies below 2 keV. Furthermore, no correlation was observed between the yield of positronium and the positron diffusion length within the sample. This suggests that the glancing angle scattering of low-energy positrons is the primary mechanism responsible for positronium formation in metal surfaces not cleaned in-situ.

topics: positronium, slow positron beam, surface

1. Introduction

Variable-energy slow-positron beams provide a unique opportunity for investigation of the interaction of low energy positrons with solid surfaces [1]. A positron is thermalized within a few ps upon implantation into a metal target [2]. The implantation profile of monoenergetic positrons can be described using the Makhovian distribution [3]. For low energy positrons, the mean penetration depth is very low, e.g., the mean penetration depth of positrons with energy of 0.5 keV in Au is ≈ 0.7 nm. Positrons that have been thermalized in the sub-surface region are capable of diffusing back to the surface. Multiple processes may occur when a thermalized positron reaches the surface:

(i) Positron re-emission. The positron work-function is defined as [4, 5]

$$\varphi_+ = -D - \mu_+, \tag{1}$$

where D is the surface dipole barrier and μ_+ is the positron chemical potential. In contrast to electrons for which the work function is positive for all metals, the positron work function for some metals (e.g., Ag, Au, Pb) is positive, while for some other metals (e.g., Al, W, Ni) it is negative. In the case of metals with negative φ_+, it is energetically more favorable for the positron to reside in a vacuum rather than inside the metal. Consequently, positrons that reach the surface are spontaneously emitted into the vacuum.

(ii) Positron trapping in the surface state. The metal surface acts as a potential well for a positron due to the image potential arising from the correlation of electrons inside the metal with a positron outside [6]. Hence, the metal–vacuum interface can be regarded as a big void. Positrons reaching the surface are trapped in the surface potential well and are annihilated there, attached to the surface in so-called "surface state" [7]. Note that positron trapping in the surface state is possible also for metals with a positive positron work-function [6].

(iii) Positronium emission. Positron can pick an electron on the surface, forming positronium (Ps) emitted from the surface to the vacuum [8, 9]. To form Ps, both the positron and the electron must be removed from the metal and bound together. Hence, the potential cfor formation of Ps [2] is given by the expression

$$\varphi_{\mathrm{Ps}} = \varphi_- + \varphi_+ - \frac{1}{2}R_\infty, \tag{2}$$

where φ_- and φ_+ denote the electron and positron work-function, respectively, and $\frac{1}{2}R_\infty = 6.8028$ eV is the Ps ground state binding energy [10]. Note that φ_{Ps} is properly called the Ps formation potential rather than the "Ps work-function", because Ps does not exist inside metals where any bound state between a positron and an electron is immediately destroyed by interaction with screening electrons. Ps is formed outside the metal in the tail of electron density, where the positron

bounds one of the electrons in a cloud of correlated screening electrons following the positron. *Ab-initio* calculations [11] conducted for a positron in a free electron gas indicate that the Ps formation becomes feasible when the electron gas density is sufficiently low, such that the radius of a sphere containing a single electron is $r_s > 6a_0$, where a_0 is the Bohr radius. Measurements of the kinetic energy spectrum of emitted Ps have demonstrated that Ps is formed suddenly, and the metal crystal is left in an excited state [12, 13]. The energy spectrum of the emitted Ps has a low energy tail finished with a sharp edge at an energy equal to the minus of the Ps formation potential ($-\varphi_{\mathrm{Ps}}$) [12, 13]. The Ps formation potential and the positron work-function differ by $\varphi_- - \frac{1}{2}R_\infty$ which is negative for all metals due to a high Ps binding energy ($\frac{1}{2}R_\infty > \varphi_-$). This makes Ps emission energetically more favorable than positron re-emission. However, it holds only far from the metal surface. Close to the metal surface the situation is modified by the image potential, and the positron has the lowest energy when it is trapped in the surface state [7].

(iv) Thermal desorption of positronium. A positron trapped in the surface state can escape the trap by picking an electron from the metal and forming Ps [14, 15]. This is a thermally activated process [14], and Ps desorption rate increases with temperature according to the Arrhenius law [15].

The processes (i–iv) are based on the diffusion of positrons, thermalized inside a metal back to the surface, and the Ps yield should, therefore, correlate with the mean positron diffusion length L_+ in the metal [16]

$$L_+ = \sqrt{D_+\tau}, \tag{3}$$

where D_+ is the positron diffusion coefficient and τ is the positron lifetime. A longer positron diffusion length results in a higher number of thermalized positrons reaching the surface and being available for Ps formation. Consequently, the Ps yield should increase with increasing positron diffusion length. The aim of this work was to examine the dependence of the Ps yield on the positron diffusion length for an untreated metal surface.

2. Experimental details

A magnetically guided continuous slow-positron beam was used in the present work. Fast positrons emitted by a ^{22}Na source with activity of 2 GBq were moderated using a well-annealed 7 μm thick W foil in transmission geometry [16]. Hence, positrons implanted into the foil thermalized there close to its opposite face, and reaching the opposite surface by diffusion are emitted to vacuum. Such moderated positrons are monoenergetic with kinetic energy of 3 eV corresponding to the positron work-function of tungsten, $\varphi_+ = -3$ eV [16]. The W foil is coupled to three W meshes with negative bias gradually increasing to -27 V. It improves the collection efficiency of moderated positrons. Because of the -27 V bias, moderated positrons in our beam have a kinetic energy of 30 eV. Moderated positrons are separated from fast ones by bending the beam tube in a magnetic field and are guided in vacuum by the magnetic field to the sample. Doppler broadening of the annihilation γ-rays is measured using a high purity germanium (HPGe) detector with an energy resolution of 1.09 keV at 511 keV. Waveforms from the HPGe detector are sampled using a 12-bit digitizer Acqiris DC440 and evaluated by applying the procedure described in [17].

The Doppler broadening of annihilation photopeak was evaluated using the line shape parameters S and W [18]. Ps can exist either as *para-positronium* (p-Ps), i.e., $^1S_0$ singlet state with total spin 0, or as *ortho-positronium* (o-Ps), i.e., $^3S_1$ triplet state with total spin 1 [10]. The formation ratio of p-Ps to o-Ps is 1:3. The p-Ps has a lifetime of 125 ps and decays by self-annihilation into 2γ-rays. In turn, o-Ps in vacuum has a lifetime more than three orders of magnitude longer, which is 142 ns, and decays into 3γ-rays [10]. In the case of the 2γ annihilation the annihilation γ-rays have an energy of 511 keV (slightly modified by Doppler shift) and contribute to the annihilation photopeak. In contrast, in the case of the 3γ annihilation the emitted γ-rays have a continuous energy spectrum [19] and contribute to the low energy region below the annihilation photopeak. Hence, the contribution of the 3γ annihilations can be easily distinguished from the 2γ annihilations. A measure of the 3γ annihilation contribution is provided by the so-called R parameter [20], defined as the ratio of the total number of counts $A_{3\gamma}$ in the low energy region below the annihilation peak to the total number of counts $A_{2\gamma}$ in the annihilation photopeak,

$$R = A_{3\gamma}/A_{2\gamma}. \tag{4}$$

As depicted in Fig. 1 the 2γ annihilation region (annihilation photopeak) corresponds to the energy interval ± 5.6 keV around 511 keV. The 3γ annihilation region was selected as the energy interval from 350 to 500 keV. It is noteworthy that the lower boundary of the 3γ annihilation region is set at 350 keV despite the presence of 3γ annihilation γ-rays with lower energies. This boundary was chosen to remain above the Compton edge of 511 keV γ-rays, thereby ensuring that the R parameter remains unaffected by background arising from the 511 keV γ-rays interacting in the detector through Compton scattering.

The energy spectra plotted in Fig. 1 were measured from a well-annealed (850°C/1 h) Au sample utilizing positrons with energies of 30 eV

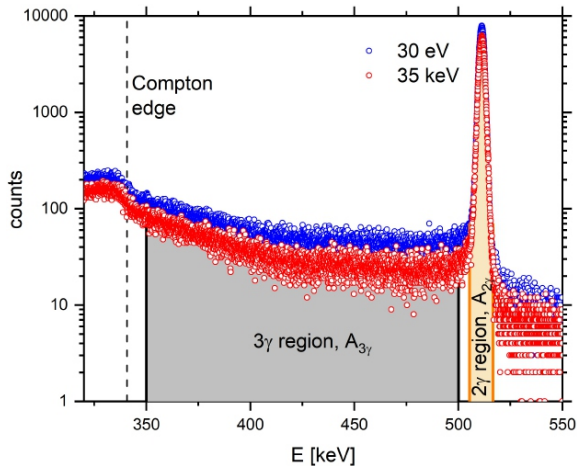

Fig. 1. Example of the γ-ray energy spectrum for the annealed Au sample measured using positrons with energy of 30 eV (blue points) and 35 keV (red points). The spectra were normalized to the same area. The regions used for calculating the R parameter are indicated by filled areas. The vertical dashed line shows the Compton edge for the 511 keV γ-rays.

and 35 keV. It is evident that the number of counts in the 3γ region below the annihilation photopeak is enhanced in the spectrum acquired with 30 eV positrons due to the 3γ annihilations of o-Ps formed on the surface. Thus, the R parameter for the spectrum measured with low-energy positrons of energy E can be expressed as

$$R(E) = \frac{\xi P_{3\gamma}(E) + \mathrm{bcg}}{P_{2\gamma}(E)}, \tag{5}$$

where $P_{2\gamma}$ represents the fraction of 2γ annihilations, $P_{3\gamma}$ denotes the fraction of 3γ annihilations multiplied by a coefficient ξ that accounts for the fact that we do not use the whole energy range of the 3γ annihilation γ-ray energy spectrum, and "bcg" describes the background from other events falling into the 3γ region.

For the spectrum measured with 35 keV positrons, the contribution of o-Ps is absent ($P_{3\gamma} = 0$) as the penetration depth of 35 keV positrons into Au is 479 nm, which makes the fraction of positrons diffusing back to the surface negligible. Therefore, the R parameter for the spectrum obtained with 35 keV positrons is given by

$$R(E{=}35\,\mathrm{keV}) = \frac{\mathrm{bcg}}{P_{2\gamma(E)}}. \tag{6}$$

By subtracting (5) and (6), the background contribution bcg is eliminated resulting in the so-called F parameter

$$F(E) = R(E) - R(E{=}35\,\mathrm{keV}) = \xi \frac{P_{3\gamma}(E)}{P_{2\gamma(E)}}, \tag{7}$$

which is directly proportional to the ratio of 3γ to 2γ annihilations. In the following text F is used as a measure of Ps yield.

3. Results and discussion

To examine the possible dependence of the Ps yield on the positron diffusion length, two Au (purity 99.99%) samples were investigated: (i) sample annealed at 800°C for 1 h vacuum and (ii) sample subjected to plastic deformation by cold rolling. No in-situ cleaning of the Au surface was done, i.e., the surface is covered by adsorbed gas molecules. The dependence of the S and W parameters measured for these Au samples is plotted in Fig. 2a and 2b, respectively. At low energies, positrons are annihilated predominantly in the surface state, resulting in similar S and W parameters for both annealed and cold-rolled samples. As the energy increases, positrons penetrate progressively deeper into the Au sample, and the fraction of positrons diffusing back to the surface decreases gradually. This trend is reflected by the S and W parameters approaching bulk values at high energies corresponding to the condition when all positrons are annihilated within the Au sample. The cold-rolled sample exhibits a significantly higher bulk value of the S parameter and a lower one of the W parameter compared to the annealed sample due to the positron being trapped at dislocations introduced by plastic deformation. The positron diffusion length L_+ was determined by fitting the dependence of the S and W parameters on the energy E of the incident positrons using the VEPFIT code [21]. The annealed sample exhibits a positron diffusion length of (118 ± 6) nm, whereas the cold-rolled sample, due to reduced positron mobility caused by trapping at dislocations, exhibits a significantly shorter positron diffusion length of (30 ± 2) nm.

Figure 2c presents the evolution of the F parameter, which provides information about the Ps yield. The dependence of F is notably similar in both annealed and cold-rolled samples despite of their differing positron diffusion lengths. The Ps formation occurs only at very low energies of incident positrons, $E < 2$ keV. At higher positron energies, F sharply decreases to zero. Note that the energy of 2 keV corresponds to a positron penetration depth in Au of ≈ 6 nm. Thus, in Au samples, Ps is formed only for very low positron energies, and the Ps yield is not affected by the positron diffusion length.

Similar results were obtained for Pd samples. Figure 3 compares (i) a well-annealed bulk Pd sample and (ii) a nanocrystalline Pd film, 490 nm thick, deposited on (100) Si substrate using cold cathode beam sputtering. Similarly to Au samples, no in-situ surface cleaning was done. The bulk Pd sample annealed at 1000°C for 1 h in vacuum contains a very low concentration of defects. In the annealed sample, most of the positrons are annihilated in the free state delocalized within the Pd lattice. The microstructure of the Pd films is described in [22] and consists of column-like grains with a mean width of ≈ 50 nm. Thus, unlike the annealed bulk Pd, the Pd

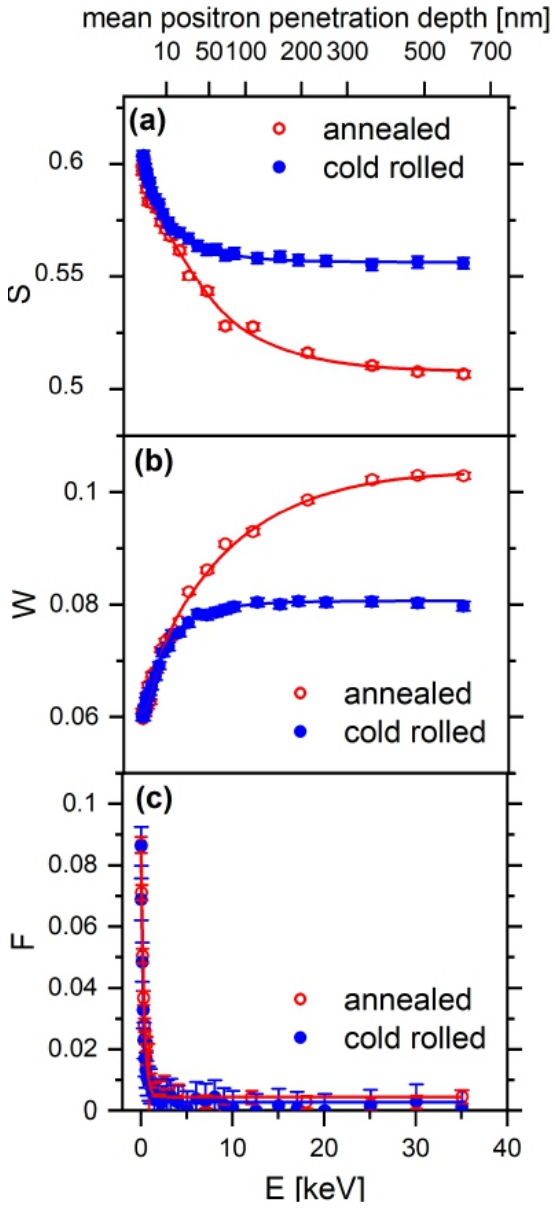

Fig. 2. Results of investigations of well-annealed and cold-rolled Au sample: (a) $S(E)$ curve; (b) $W(E)$ curve; (c) $F(E)$ curve. Solid lines in panels (a–b) are model curves calculated using the VEPFIT code [21]. Solid lines in the panel (c) were obtained by fitting of experimental points using (8). The upper x-axis shows the mean positron penetration depth.

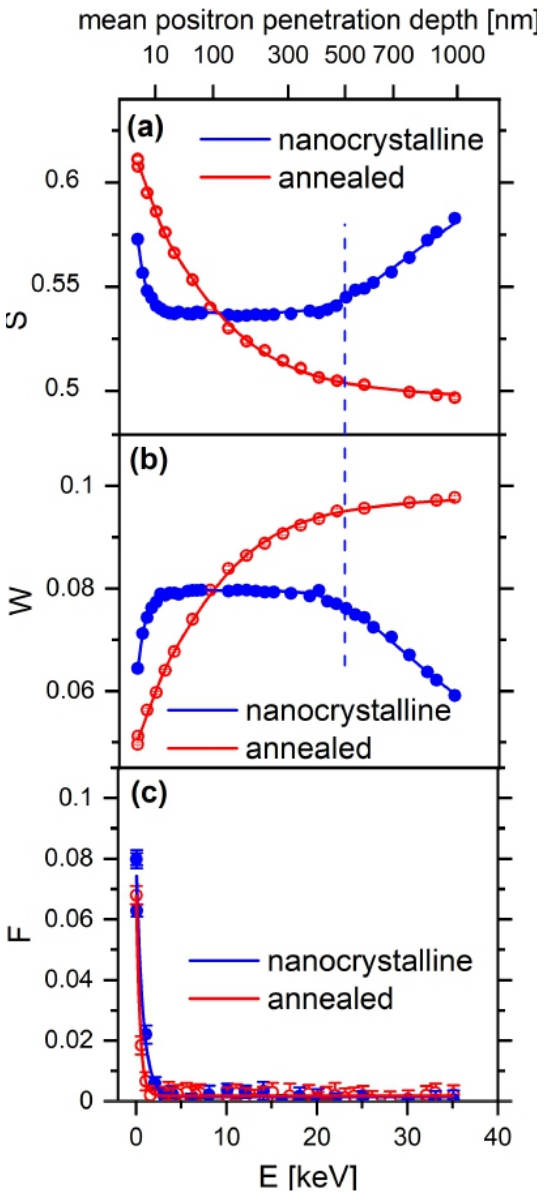

Fig. 3. Results of investigations of well-annealed bulk Pd sample and nanocrystalline Pd film: (a) $S(E)$ curve; (b) $W(E)$ curve; (c) $F(E)$ curve. Solid lines in panels (a–b) are model curves calculated using the VEPFIT code [21]. Solid lines in the panel (c) were obtained by fitting of experimental points using (8). The upper x-axis shows the mean positron penetration depth. The vertical dashed line indicates the position of the interface between Pd film and Si substrate.

film contains a high concentration of lattice defects, and the majority of positrons are annihilated in the trapped state in the open volume defects at the grain boundaries. This is evidenced by the higher S and lower W parameters of the Pd film compared to the annealed bulk Pd. At energies above 23 keV, positrons penetrate into the Si substrate leading to a further increase in S and a decrease in W. The annealed sample exhibits a positron diffusion length of (151 ± 4) nm, while the nanocrystalline Pd film shows a significantly reduced positron diffusion length of (10 ± 2) nm. Figure 3c demonstrates that despite the markedly different positron diffusion lengths, the F parameter curves for both Pd samples are nearly identical. As with Au samples, the Ps formation occurs only at very low incident positron energies, with F rapidly decreasing to zero as the positron energy increases.

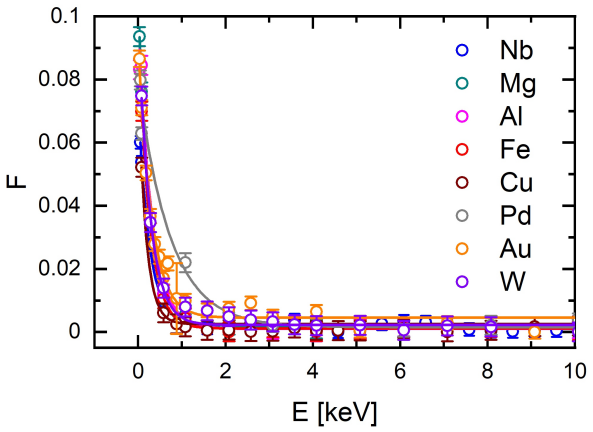

Fig. 4. The F parameter curves for various annealed metals. The solid lines are model curves obtained from fitting the experimental points using (8).

Figure 4 compares the F parameter curves for various annealed bulk metals, revealing a clear similarity in their development. For all metal samples studied, Ps formation occurs only at very low positron energies, with the Ps contribution rapidly diminishing as the energy of incident positrons increases. The dependence of the F parameter on the positron energy is well described by a simple exponential curve

$$F(E) = F_0 \exp\left(-\frac{E}{E_0}\right). \tag{8}$$

The parameters E_0 obtained from fitting of the $F(E)$ curves by (8) for the annealed metals are collected in Table I. The mean positron penetration depths d_0 corresponding to the E_0 energies calculated using the Makhovian implatation profile [3] are also listed in Table I. The E_0 values for the various metals are very similar, not exceeding 0.5 keV. The corresponding d_0 values are higher for samples with a lower density and do not exceed 2.5 nm for any of the studied samples. For comparison, Table I also presents the positron diffusion lengths L_+ obtained from fitting the $S(E)$ curves of each metal sample. Clearly, the values of d_0 are independent of L_+, with the positron diffusion length being roughly two orders of magnitude longer than d_0.

The measured data indicate no correlation between the Ps yield and the positron diffusion length. Neither Ps emission from the surface nor thermal desorption of Ps can explain these results, because both these mechanisms of Ps formation assume back-diffusion of thermalized positrons to the surface, implying that the Ps yield must depend on the positron diffusion length in the sample. The only plausible explanation is Ps formation via an alternative mechanism. Gidley at el. [23] demonstrated that Ps can form through glancing-angle scattering of low-energy positrons on the metal surface. This mechanism is fundamentally different because

TABLE I

Parameters E_0 obtained by fitting the F parameter curves measured for various annealed metals using (8). The positron penetration depth d_0 corresponds to the energy E_0. For comparison the mean positron diffusion length L_+ obtained from fitting the S and W parameter curves using the VEPFIT code [21] is shown in the last column of the table.

Sample	Annealing	E_0 [keV]	d_0 [nm]	L_+ [nm]
Mg	450°C/1 h	0.24(1)	2.3(1)	200(30)
Al	450°C/1 h	0.31(3)	2.2(2)	240(10)
Fe	1000°C/1 h	0.26(1)	0.59(3)	169(5)
Cu	850°C/1 h	0.18(4)	0.29(8)	180(20)
Nb	1000°C/1 h	0.25(3)	0.51(6)	180(10)
Pd	1000°C/1 h	0.49(8)	1.1(2)	150(10)
W	1800°C/1 h	0.27(2)	0.26(3)	190(10)
Au	850°C/1 h	0.31(2)	0.32(3)	118(6)

Ps is formed by non-thermalized positrons entering the metal surface *from outside* at low angles of incidence. Some of these incident positrons are quasi-elastically scattered on the surface, simultaneously capturing an electron from the conduction band to form Ps. Thus, the Ps yield strongly depends on the energy and angle of incidence of the incoming positrons but is completely independent of the positron diffusion length in the sample. Gidley et al. [23] observed a sharp increase in the Ps yield at low angles of incidence. In our experiment, conducted using a magnetically guided slow-positron beam, positrons enter the sample at various angles of incidence. At low positron energies, the transverse component of the positron momentum can exceed the longitudinal component, causing positrons to strike the sample at glancing angles of incidence. At higher positron energies, the longitudinal component of positron momentum becomes much greater than the transverse component, resulting in positron impacting the sample nearly perpendicular to the surface, making the Ps formation by glancing-angle scattering improbable. Therefore, we conclude that glancing-angle scattering of low-energy positrons is the primary source of Ps observed in our experiment. The majority of positrons that thermalize inside the sample and diffuse back to the surface are trapped in the surface potential well and annihilated in the surface state, thus not contributing to the formation of Ps. This conclusion aligns with theoretical modeling, which shows that although the Ps formation potential is smaller than the positron work-function, the positron localization in the surface state near the metal surface is energetically more favorable than the Ps formation [6].

It should be mentioned that no in-situ surface treatment of metal samples was done in our experiment. In contrast, Mills et al. [13] cleaned the sample surface prior to measurement by bombarding it with 1 keV Ar^+ ions followed by in-situ annealing in ultrahigh vacuum (UHV). Additionally, the positron beam they used was electrostatically guided to ensure perpendicular incidence of positrons on the sample surface. In our experiment, the sample surfaces were covered with adsorbed gas molecules, likely deepening the surface potential well and increasing the probability of positron trapping in the surface state.

4. Conclusions

Our investigations using a magnetically guided slow positron beam revealed that glancing-angle scattering of low-energy positrons is the predominant mechanism of Ps formation on untreated metal surfaces at ambient temperature. This is because most thermalized positrons diffusing back to the surface are trapped in the surface state. Measurements of various metal samples revealed that Ps is formed only at very low positron energies ($E < 2$ keV) with the Ps contribution decreasing abruptly as the energy of incident positrons increases. The Ps yield is not influenced by the positron diffusion length in the sample.

References

[1] C. Hugenschmidt, *Surf. Sci. Reports* **71**, 547 (2016).

[2] M.J. Puska, R.M. Nieminen, *Rev. Mod. Phys.* **66**, 841 (1994).

[3] A.F. Makhov, *Sov. Phys. Solid State* **2**, 1934 (1961).

[4] R.M. Nieminen, C.H. Hodges, *Solid State Comm.* **18**, 1115 (1976).

[5] C.H. Hodges, M.J. Stott, *Phys. Rev. B* **7**, 73 (1973).

[6] C.H. Hodges, M.J. Stott, *Solid State Comm.* **12**, 1153 (1973).

[7] P.A. Huttunen, J. Mäkinen, D.T. Britton, E. Soininen, A. Vehanen, *Phys. Rev. B* **42**, 1560 (1990).

[8] K.F. Canter, A.P. Mills Jr., S. Berko, *Phys. Rev. Lett.* **33**, 7 (1974).

[9] A.P. Mills Jr., L. Pfeiffer, P.M. Platzman, *Phys. Rev. Lett.* **51**, 1085 (1983).

[10] S.D. Bass, S. Mariazzi, P. Moskal, E. Stępień, *Rev. Mod. Phys.* **95**, 021002 (2023).

[11] D.N. Lowy, A.D. Jackson, *Phys. Rev. B* **12**, 1689 (1975).

[12] A.P. Mills, Jr., L. Pfeiffer, P.M. Platzman, *Phys. Rev. Lett.* **51**, 1085 (1983).

[13] A.C.L. Jones, H.J. Rutbeck-Goldman, T.H. Hisakado, A.M. Piñeiro, H.W.K. Tom, A.P. Mills, Jr., B. Barbiellini, J. Kuriplach, *Phys. Rev. Lett.* **117**, 21640 (2016).

[14] A.P. Mills, Jr., *Phys. Rev. Lett.* **41**, 1828 (1978).

[15] A.P. Mills, Jr., E.D. Shaw, M. Leventhal, R.J. Chichester, D.M. Zuckerman, *Phys. Rev. B.* **44**, 5791 (1991).

[16] P.J. Schultz, K.G. Lyn, *Rev. Mod. Phys.* **60**, 70 (1988).

[17] J. Čížek, M. Vlček, I. Procházka, *Nucl. Instrum. Meth. in Phys. Res. A* **623**, 982 (2010).

[18] P. Coleman, *Positron Beams and Their Applications*, Word Scientific, p. 340, (2000).

[19] D. Kamińska, A. Gajos, E. Czerwiński et al., *Europ. Phys. J. C* **76**, 44 (2016).

[20] Y.C. Wu, J. Jiang, S.J. Wang, A. Kallis, P.G. Coleman, *Phys. Rev. B* **84**, 06412 (2011).

[21] A. van Veen, H. Schut, M. Clement, J.M.M. de Nijs, A. Kruseman, M.R. IJpma, *Appl. Surf. Sci.* **85**, 216 (1995).

[22] J. Čížek, O. Melikhova, M. Vlček, F. Lukáč, M. Vlach, I. Procházka, W. Anwand, G. Brauer, A. Mücklich, S. Wagner, H. Uchida, A. Pundt, *Int. J. Hydrogen Energy* **38**, 12115 (2013).

[23] D.W. Gidley, R. Mayer, W.E. Frieze, K.G. Lynn, *Phys. Rev. Lett.* **58**, 59 (1987).